FPGA Contribution in Photovoltaic Pumping Systems: Models of MPPT and DTC-SVM Algorithms

Saber KRIM*‡, Soufien GDAIM**, Abdellatif MTIBAA***, and Mohamed Faouzi MIMOUNI****

* Department of Electrical and Automatic, Polytechnic School of Sousse, University of Sousse, BVD Khalifa KAROUI 4054 Sahloul – Sousse, Tunisia

**Department of Informatics, Higher Institute of Informatics, University of Monastir, Avenue Habib Bourguiba, Sidi Massoud -BP 49 Mahdia 5111, Tunisia

***Department of Electrical Engineering, National Engineering School of Monastir, Laboratory of Electronics and Microelectronics of the FSM, Avenue Ibn El Jazzar, 5019, University of Monastir, Tunisia

****Department of Electrical Engineering, National Engineering School of Monastir, Research Unit of industrial systems Study and renewable energy (ESIER), Avenue Ibn El Jazzar, 5019, University of Monastir, Tunisia

(krimsaber@hotmail.fr, sgdaim@yahoo.fr, abdellatif.mtibaa@enim.rnu.tn, Mfaouzi.mimouni@enim.rnu.tn)

‡Corresponding Author, Avenue Ibn El Jazzar, Monastir 5019, Tunisia,

Tel: +216 95 199 953, krimsaber@hotmail.fr

Received: 24.03.2016 Accepted:01.06.2016

Abstract- This paper aims to propose and develop a research platform which can be utilized for rapid prototyping of control algorithms of power converters used in the field of renewable energy, such as the photovoltaic systems. This study investigates the use of the Field-Programmable Gate Array (FPGA) to control the DC/DC power converter and the voltage inverters used in solar photovoltaic pumping systems. The power circuit of the pumping system consists of a PV system, a DC/DC converter, a two-level voltage inverter and an induction motor. The control system is based on an MPPT control algorithm and a Direct Torque Control with a Space Vector Modulation (DTC-SVM) based on proportional-integral controllers. In order to perform the hardware in the loop, the power circuit is realized using the Simulink blocks and the control system is designed using the Xilinx System Generator (XSG) tool. The VHDL code and the bit stream file of the suggested control algorithms have been automatically generated using the XSG tool. The hardware co-simulation step is carried out in the laboratory utilizing an FPGA Virtex 5 ML 507 and the Matlab/Simulink environment. A comparative study between the classical DTC and the DTC-SVM is presented. The FPGA-performance in terms of computation power is demonstrated.

Keywords Photovoltaic, water pumping, DTC-SVM, MPPT, FPGA.

1. Introduction

Solar energy is widely used to feed the isolated regions and the deserted areas, which is essentially utilized for lighting, charging batteries, pumping, etc... The great advantage is that this source is exhaustible, offers a security in use and it is clean for the environment. Predominantly for these regions, the water presents the main factor in development, which can be used in irrigation and the individual needs. To access the water, the pumping systems connected to the electrical grid can be utilized, which requires an expensive investment due to the great distance between these regions and the town center. To solve this problem, the photovoltaic (PV) pumping systems can be used such as an economic and efficient solution [1]. This solution has been investigated and commercialized for the last few years, as an important idea to improve the robustness and reduce the cost [2].

In the last years, the pumping systems have been based on DC motors to convert the electrical energy produced by the PV system to a mechanical energy to train the pumps. The DC motors are featured by their control simplicity and direct connection to the PV through a DC/DC converter. However, the main limitation of these motors is that the maintenance rate is very important because of the existence of a brushes'commutator system, which reduces the system yield. Recently, the Induction Motors (IMs) are frequently used in several industrial applications thanks to their low maintenance, low cost and simple control [3, 4]. In this paper an IM is utilized in the pumping system and controlled by the Direct Torque Control (DTC). The DTC is becoming a more used approach in the industrial applications thanks to its rapid dynamic response, its simple structure and its robustness under various motor parameters [5, 6]. Nevertheless, the classical DTC approach suffers from a high stator current distortion, torque ripples and a variation in the switching frequency. This reduces the pumping system performances and its lifespan. The classical DTC limitation is caused by to the two hysteresis controllers used to control both the stator flux and the electromagnetic torque [7]. Several methods have been utilized to overcome the conventional DTC disadvantages, such as the use of a multi-level inverter [8], but this method increases the cost of the inverter. Another method is based on the intelligent technique, like the neural networks and the fuzzy logic, but in this method the switching frequency remains variable and does not provide a good performance in terms of torque and flux ripples [9, 10]. In the DTC, with a constant switching frequency, the ripples can be enormously reduced. In this article, the Space Vector Modulation (SVM) is used to fix the switching frequency and improve the DTC performances. The DTC, based on the SVM, is referred to as the DTC-SVM. To reach the peak power a DC/DC, converter must be used and installed between the PV Generator (PVG) and the load. The power adjustment is realized with the variation of the duty cycle of the DC/DC converter.

Therefore, in order to get the maximum of power from the PV panel output, the duty cycle must be generated through the Maximum Power Point Tracking (MPPT) algorithms [11, 12]. Recently, several MPPT algorithms have been developed in the literature [13, 14], such as the Fractional Short Circuit Current [15], the Fractional Open Circuit Voltage [16, 17], the Perturb and Observe (P&O) [18–22], the Incremental Conductance (IC) [23-25, 26], the Hill Climbing (HC) algorithm [27], The MPPT based on the Fuzzy Logic Control (FLC) [28], the Artificial Neural Network (ANN) [29], the Genetic Algorithm (GA) [30], and the Particle Swarm Optimization (PSO) [31]. In Open Circuit Voltage, the operating point is close to the MPP when the PV voltage is about 76% of the open circuit voltage [32]. The Perturb and Observe (P&O) MPPT method operates with the voltage perturbation based on the actual and previous power values. In paper [33], a comparative study in terms of efficiency between some MPPT algorithms was presented. It was shown that P&O is the most common algorithm used in commercial converters [34]. The IC had a performance level close to the P&O, but in general the higher implementation cost compared to P&O would not be justified by an improvement in performance [33]. In [35], some MPPT techniques were investigated. It was found that the P&O and HC were featured by their simplicity in implementation. On the other hand, the IC has been slightly more complex relative to the P&O method. For this reason, the P&O method is chosen in this paper.

The suggested approach is known as a complex control algorithm that requires digital devices with a high processing speed. Conventionally, the digital controllers like the STM microcontrollers (STM32F3, STM32F4, STM32F1…) and the Digital Signal Processors (DSPs) are so much utilized to implement the control algorithm of the IM and the PV systems [36, 37]. Nevertheless, the main limitation of these digital controllers is the low computational power, owing to their sequential computations, which needs a high sampling period, thus creating a delay in applying the inverter switching states. This increases the commutation losses and then raises the stator current distortion [38]. To overcome these solution limitations, an alternative solution can be chosen, such as the FPGA, which is featured by a high computation power thanks to its parallel processing [10, 38, 39].

Configuring the FPGAs, a VHSIC Hardware Description Language (VHDL) is necessary, but programming the VHDL needs the knowledge of the VHDL instructions and an important development time. To face out this problem, the Xilinx System Generator (XSG) tool is offered for as a low cost solution to design, simulate and automatically generate the VHDL code with a rapid prototyping and without any knowledge of the Hardware Description Language (HDL) [40].

2. Theory

The diagram of the pumping photovoltaic system is given by Fig. 1. The DC/DC converter is controlled through an MPPT algorithm. The IM is controlled by the DTC approach.

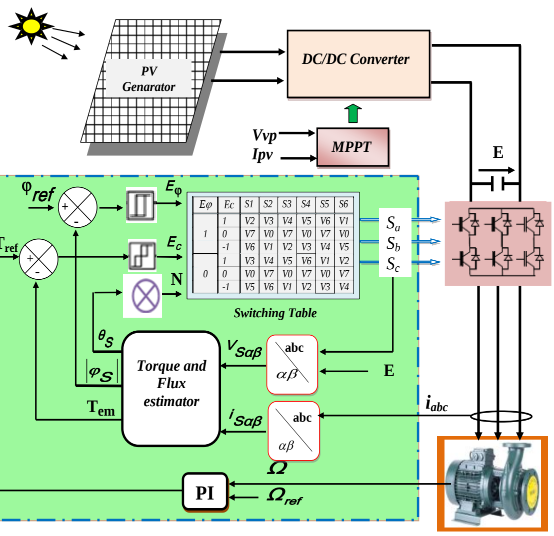

Fig. 1. Pumping photovoltaic system diagram based on DTC

The system presented in Fig.1 is based on the classical DTC, which produces a torque and flux with high ripples and feeds the IM by a current with high distortions. To cope with the DTC limitations, a pumping photovoltaic system based on the DTC-SVM is proposed and represented in Fig. 2.

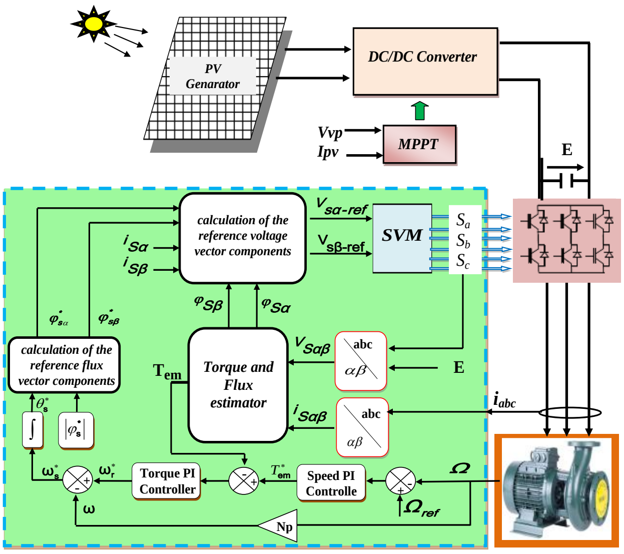

Fig. 2. Pumping photovoltaic system diagram based on DTC-SVM

2.1. Photovoltaic system

The model of the PV cell based on a single diode is illustrated in Fig.3 and used in this study, thanks to its simplicity relative to other models based on double or three diodes [41-44]. The utilized model is shown in Fig. 3, which consists of four components: a current generator Iph, a diode, a parallel resistance Rsh and a serial resistance Rs [45]. The current obtained by one cell is very weak, which necessitates being associated in parallel with Np cells and in serial with Ns cells to increase the voltage and then raise the PV power. The Np and Ns cells form a PV module.

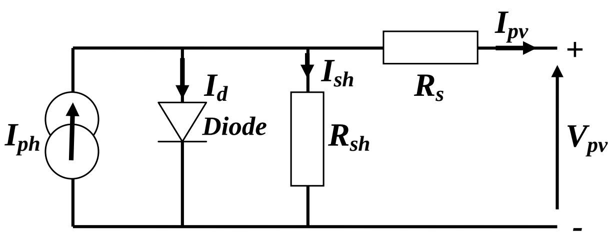

Fig. 3. Model of PV cell based on single diode

The output current Ipv is given by the following expression:

$$I_{pv} = I_{ph} - I_d - I_{sh} \tag{1}$$

The current obtained by the PV module is given by equation (2):

$$I = N_p I_{ph} - N_p I_0 \left(e^{q\left(\frac{V_{pv}+R_s I}{akTN_s}\right)} - 1\right) - \frac{V_{pv}+R_s I}{R_{sh}} \tag{2}$$

with:

I: the current in the load

Vpv: the output voltage

Iph: the generated current of the photo cell

Rs: the serial resistance

Rsh: the shunt resistance

I0: the reverse saturation current of the diode

a (1≤a≤ 1.5): ideal factor of the PV

k= 1.38 10-23 J/K: constant of Boltzmann

q= 1.6 10-19 C: Electron quantity.

On the one hand, the physical behavior of the PV generator is depends on Rs, Rsh, Ipv and I0. On the other hand, the PV cell is sensitive to the weather variation, like the solar radiation and the temperature [44].

2.2. DC/DC power converter model and MPPT algorithm

The voltage regulator is presented by a boost converter, which is supplied by the power generated by the PV module, as shown in Fig. 4. This converter is based on a power transistor (IGBTs or MOSFETs) controlled by a pulse width modulation signal. The control algorithm is based on an MPPT controller [43, 45].

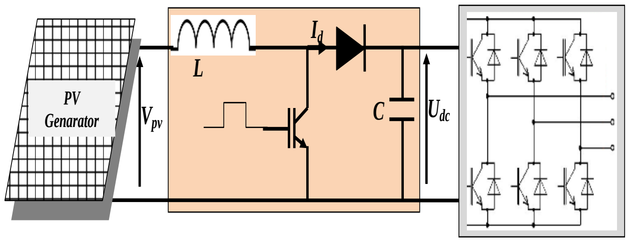

Fig. 4. Structure of DC-DC converter

The relationship between the voltages Udc and Vpv is given by the following equation [46]:

$$U_{dc} = \frac{1}{1-\alpha} V_{pv} \tag{3}$$

where α is the duty cycle.

In this paper the duty cycle is generated through the P&O method. Thanks to its simplicity, the P&O method is mostly used to research the MPPT because it is an iterative method and requires only the acquisition of (Vpv, Ipv). It can track the maximum power point even during sudden changes' irradiation and temperature. As its name suggests, the P&O method is based on the disruption of the Vpv voltage and the observation of this change impact on the power output of the photovoltaic panel. The principle of this method is illustrated in the following figure. [12, 47].

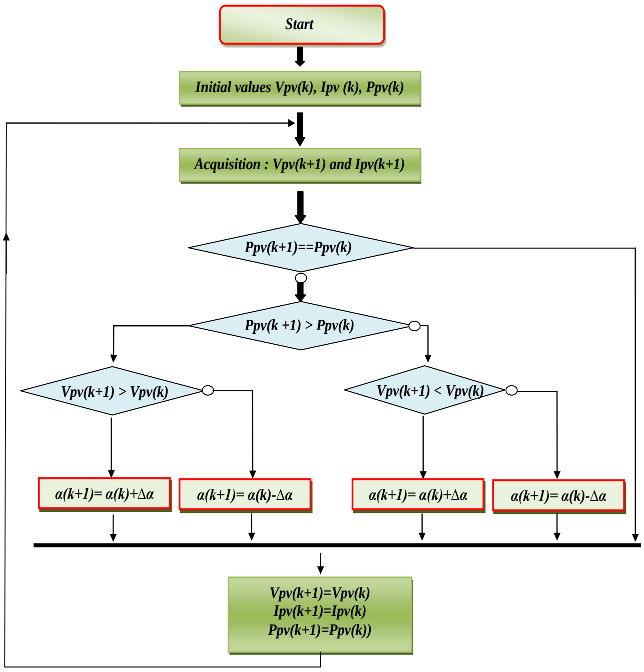

Fig. 5. MPPT control algorithm diagram

This controller consists in generating a perturbation so as to increase or decrease the duty cycle of the PWM and show its affect on Ppv [48].

2.3. *Conventional DTC principle*

The system of equations (4) describes the IM model in the Concordia reference:

$$\begin{cases} \frac{d\varphi_{s\alpha}}{dt} = v_{s\alpha} - R_s\, i_{s\alpha} \\ \frac{d\varphi_{s\beta}}{dt} = v_{s\beta} - R_s\, i_{s\beta} \\ \frac{d\varphi_{r\alpha}}{dt} = -R_r\, i_{r\alpha} - \omega\varphi_{r\beta} \\ \frac{d\varphi_{r\beta}}{dt} = -R_r\, i_{r\beta} + \omega\varphi_{r\alpha} \end{cases} \quad (4)$$

with:

- $\overline{v_s} = \left(v_{s\alpha}\; v_{s\beta}\right)^T$: voltage vector components
- $\overline{\varphi_s} = \left(\varphi_{s\alpha}\; \varphi_{s\beta}\right)^T$: stator flux vector components
- $\overline{\varphi_r} = \left(\varphi_{r\alpha}\; \varphi_{r\beta}\right)^T$: rotor flux vector components.
- $\overline{i_s} = \left(i_{s\alpha}\; i_{s\beta}\right)^T$: stator current vector components
- R_s, R_r : stator and rotor resistances respectively.

The mechanical behavior of the IM is described by the following equations:

$$\begin{cases} J\frac{d\Omega}{dt} = T_e - T_l - f\Omega \\ T_{em} = \frac{3}{2} N_p \left(\varphi_{s\alpha} i_{s\beta} - \varphi_{s\beta} i_{s\alpha}\right) \end{cases} \quad (5)$$

where Tem is the electromagnetic torque, Tl is the load torque, and Np, f and J are the pairs-pole number, the viscous friction coefficient and the rotor inertia, respectively.

The three-phase to two-phase transformation of the stator current is presented as follows:

$$\begin{cases} i_{s\alpha} = \sqrt{\frac{3}{2}}\, i_{sa} \\ i_{s\beta} = \frac{1}{\sqrt{2}}\left(i_{sb} - i_{sc}\right) \end{cases} \quad (6)$$

To estimate the stator flux, the following relationship can be used:

$$\begin{cases} \varphi_{s\alpha} = \int\left(v_{s\alpha} - R_s i_{s\alpha}\right)dt \\ \varphi_{s\beta} = \int\left(v_{s\beta} - R_s i_{s\beta}\right)dt \end{cases} \quad (7)$$

Utilizing the inverter switching states (Sa, Sb, Sc), the voltage vector components ($v_{s\alpha}, v_{s\beta}$) can be estimated as:

$$\begin{cases} v_{s\alpha} = \frac{2}{3} E\left(S_a - \frac{S_b - S_c}{2}\right) \\ v_{s\beta} = \frac{2}{3} E \frac{S_b - S_c}{\sqrt{3}} \end{cases} \quad (8)$$

As depicted in Fig. 1, the basic DTC structure is based on two hysteresis controllers, which are used to control the stator flux and the electromagnetic torque. The stator flux hysteresis controller is given in Fig.6. This controller presents the stator flux error as an input and a logical decision Kφ as an output.

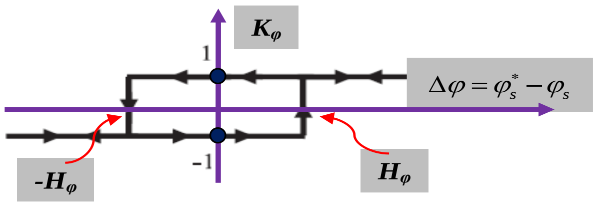

Fig. 6. Two-level hysteresis controller of stator flux

The electromagnetic torque hysteresis controller is illustrated in Fig.6. This controller shows the electromagnetic error as an input and a logical decision KT as an output.

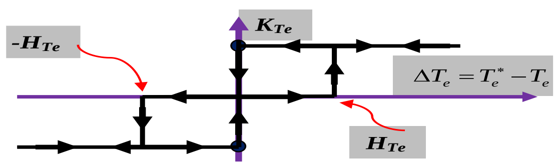

Fig. 7. Three-level hysteresis controller of torque

- If $K_{\varphi}=1 and\ K_T=1$, a rise of the flux is required.
- If $K_{\varphi}=-1 and\ K_T=-1$, a decrease in flux is needed.
- If $K_T=0$, the torque remains constant.
- $\left[-H_{\varphi},\ H_{\varphi}\right]$:is the hysteresis band of the stator flux.
- $\left[-H_{T_e},\ H_{T_e}\right]$: is the hysteresis band of the electromagnetic torque.

The stator flux position is calculated using equation (9):

$$\theta_s = arctg\left(\frac{\varphi_{s\beta}}{\varphi_{s\alpha}}\right) \quad (9)$$

In the classical DTC, the (α, β) reference is subdivided into six sectors, Si(i=1...6), as indicated in Fig. 8. Opening up the sector is defined by an angle equal to 60° [49]. Each sector is divided by a voltage vector in two equal parts, as demonstrated in Fig.8.

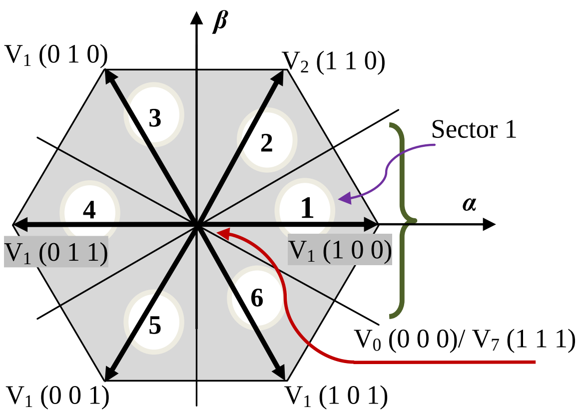

Fig. 8. Sectors and voltage vectors

For each sampling, period the voltage vector is chosen according to two hysteresis controller decisions and to the number of the sector when the stator flux is located.

Table 1. Switching table

K_{φ}	K_C	S1	S2	S3	S4	S5	S6
	1	V2	V3	V4	V5	V6	V1
1	0	V7	V0	V7	V0	V7	V0
	-1	V6	V1	V2	V3	V4	V5
	1	V3	V4	V5	V6	V1	V2
0	0	V0	V7	V0	V7	V0	V7
	-1	V5	V6	V1	V2	V3	V4

For each sampling time, the selected voltage vector is calculated using the following equation:

$$V_S = \sqrt{\frac{2}{3}} U_{dc}\left(S_A + S_B e^{j\frac{2\pi}{3}} + S_C e^{j\frac{4\pi}{3}}\right) \quad (10)$$

where (SA, SB, SC) and U_{dc} are the switching states and the DC voltage of the inverter respectively.

2.4. DTC-SVM-based PI controllers

a- SVM Concept

The SVM is a good technique that can be used to control the voltage inverter, with less harmonic and commutation losses [50]. Fig.9 describes the position of the generated voltage vectors for each sampling period. There are eight voltage vectors from V0 to V7. As presented in this figure, each voltage vector is generated through the inverter switching states.

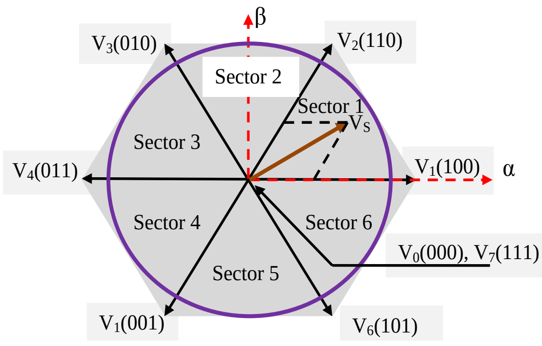

Fig. 9. Voltage vectors

As shown in Fig. 8, the determination of the voltage vector consists in projecting this vector on the two nearest adjacent vectors, as indicated in sector 1. Equation (11) can be utilized to determine the sector number and the voltage vector position.

$$\theta_S = \arctan\left(\frac{V_{S\beta}}{V_{S\alpha}}\right) \quad (11)$$

The commutation times of the inverters Ti and Ti+1 can be calculated using the components (Vsα, Vsβ) of the inverter. For example, for sector 1, the commutation times, the voltage vectors and the cyclic reports are expressed in system (12):

$$\begin{cases} \vec{V}_S = V_{S\alpha} + jV_{S\beta} = \dfrac{T_1}{T_{mod}}\vec{V}_1 + \dfrac{T_2}{T_{mod}}\vec{V}_2 \\ \vec{V}_1 = \sqrt{\dfrac{2}{3}}E\left(\cos(0) + j\sin(0)\right) = \sqrt{\dfrac{2}{3}}E \\ \vec{V}_2 = \sqrt{\dfrac{2}{3}}E\left(\cos\left(\dfrac{\pi}{3}\right) + j\sin\left(\dfrac{\pi}{3}\right)\right) \\ T_{mode} = T_1 + T_2 + T_0 \\ T_1 = \left(\sqrt{\dfrac{3}{2}}V_{S\alpha} - \dfrac{1}{\sqrt{2}}V_{S\beta}\right)\dfrac{T_{mod}}{E} \\ T_2 = \sqrt{2}V_{S\alpha}\dfrac{T_{mod}}{E} \\ D_1 = \sqrt{\dfrac{3}{2}}\dfrac{V_{S\alpha}}{E} - \dfrac{1}{\sqrt{2}}\dfrac{V_{S\beta}}{E} \\ D_2 = \sqrt{2}\dfrac{V_{S\beta}}{E} \end{cases} \quad (12)$$

Figure 10 demonstrates the space sector in sector N1. The time duration of each nonzero vector is equally divided into two parts. The time duration of the zero vectors is equally distributed from V0 to V7, and thus the switching sequence of the space vector is V0, V1, V2, V7, V7, V2, V1, and V0 during the period modulation.

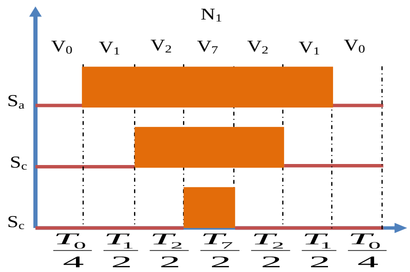

Fig. 10. Sequences of inverter switching states in sector one (N1)

The duties of the three phases of the inverter are expressed as follows:

$$\begin{cases} D_a = D_1 + D_2 + \frac{1}{2} D_0 \\ D_b = D_2 + \frac{1}{2} D_0 \\ D_c = \frac{1}{2} D_0 \\ D_1 + D_2 + D_0 = 1 \end{cases} \quad (13)$$

Referring to expressions D1 and D2 presented in system (12), system (13) can be rewritten as given by system (14):

$$\begin{cases} D_a = \frac{1}{2}\left(1 + \sqrt{\frac{3}{2}} \frac{V_{S\alpha}}{E_0} + \frac{1}{\sqrt{2}} \frac{V_{S\beta}}{E_0}\right) \\ D_b = \frac{1}{2}\left(1 - \sqrt{\frac{3}{2}} \frac{V_{S\alpha}}{E_0} + \frac{1}{\sqrt{2}} \frac{V_{S\beta}}{E_0}\right) \\ D_c = \frac{1}{2}\left(1 - \sqrt{\frac{3}{2}} \frac{V_{S\alpha}}{E_0} - \frac{1}{\sqrt{2}} \frac{V_{S\beta}}{E_0}\right) \end{cases} \quad (14)$$

b- *Concept of DTC-SVM-based PI controllers*

This control strategy ensures the decoupling between the stator flux vectors amplitude and its arguments. Indeed, the stator flux amplitude will be imposed. Nevertheless, the argument is calculated to obtain high performances like the reduction of the stator flux and the electromagnetic torque ripples. The structure of this control strategy is given by Fig.2. The difference between the conventional DTC and this control strategy is that the latter is based on the PI controllers and the SVM in order to fix the switching frequency, which consequently reduces the stator flux and the torque ripples as well as the harmonic waves of the stator current. The switching table (Takahashi.I) and the hysteresis regulators used in the conventional DTC are eliminated. The voltage vector is calculated utilizing a predictive controller. The predictive controller block's inputs are the components of the stator flux's reference, the component of the estimated stator flux vector and the components of the stator current.

- **Torque controller**

Referring to equation (15), the torque expression is based on the rotor flux vector, the stator flux vector and few motor parameters.

$$T_{em} = N_p \frac{M}{L_s L_r - M^2} \overrightarrow{\varphi_S}\, \overrightarrow{\varphi_r} \quad (15)$$

Equation (16) shows the relationship between the stator and rotor fluxes.

$$\frac{d}{dt}\overrightarrow{\varphi_r} = \frac{R_r M}{L_r L_s \sigma}\overrightarrow{\varphi_s} + \left(j\omega - \frac{R_r}{L_r \sigma}\right)\overrightarrow{\varphi_r} \quad (16)$$

Based on the Laplace transformation, equation (16) becomes:

$$\overrightarrow{\varphi_r}(p) = \frac{\frac{M}{L_s}}{\sigma \frac{L_r}{R_r} p + \left(1 - j\omega\sigma \frac{L_r}{R_r}\right)} \overrightarrow{\varphi_s}(p) \quad (17)$$

The expression of the stator flux in an exponential form is presented by equation (18).

$$\overrightarrow{\varphi_s} = \left|\varphi_s^*\right| e^{j\theta_s} = \left|\varphi_s^*\right| e^{j\omega_s t} \quad (18)$$

where $\theta_s = \omega_s t$ is the position of the stator flux vector.

Based on the Laplace transformation, equation (18) becomes:

$$\varphi_s(p) = \frac{1}{p - j\omega_s}\left|\varphi_s^*\right| \quad (19)$$

Using equations (17) and (19), after calculation and simplification, the rotor flux's temporal expression can be as below:

$$\varphi_r = \frac{M}{L_s}\left|\varphi_s^*\right| \sqrt{\frac{1 + e^{\frac{-2t}{\tau}} - 2e^{\frac{-t}{\tau}}\cos(\omega_r t)}{1 + (\tau\omega_r)^2}} \times \exp\left(j\left[\arctan\left(\frac{u}{v}\right) - \arctan(\tau\omega_r)\right]\right) \quad (20)$$

with:

$$\begin{cases} \omega_r = \omega_s - \omega \\ \tau = \sigma \frac{L_r}{R_r} \\ u = \cos(\omega_s t) - e^{-\frac{t}{\tau}}\cos(\omega t) \\ v = \sin(\omega_s t) - e^{-\frac{t}{\tau}}\sin(\omega t) \end{cases} \quad (21)$$

Replacing equations (18) and (20) in equation (15), the electromagnetic expression can be reduced and rewritten as [51]:

$$T_{em} = N_p \frac{M^2}{L_s^2 R_r} \left|\varphi_s^*\right|^2 \left(1 - e^{-\frac{t}{\tau}}\right) \omega_r \tag{22}$$

Referring to equation (22), the dynamic behavior of the electromagnetic torque is sensitive to ω_r when the reference of the stator flux is constant. Because of the linearity relationship between the electromagnetic torque and the stator flux, a PI controller can be used to control the electromagnetic torque that reduces the error between the estimated torque and the reference electromagnetic one. As presented in Fig.2, the PI torque controller provides the torque error as an input and the reference pulsation ω_r^*. The Laplace transformation of equation (22) is given by the transfer function represented by (23):

$$H(p) = \frac{T_{em}}{\omega_r} = N_p \frac{M^2}{L_s^2 R_r} \left|\varphi_s^*\right|^2 \frac{1}{1+\tau p} \tag{23}$$

The transfer function of the proposed controller is given by (24):

$$C(p) = A.\frac{1+T_i p}{T_i p} \tag{24}$$

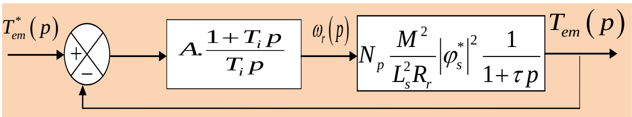

Fig. 11. Electromagnetic torque control loop

Referring to the poles' compensation method and after mathematical development and simplification, the parameters of the PI controller are given by equation (25).

$$\begin{cases} T_i = \tau \\ A = \dfrac{\zeta}{N_p \dfrac{M^2}{L_s^2 R_r} \left|\varphi_s^*\right|^2} \end{cases} \tag{25}$$

The components $\varphi_{s\alpha}^*$ and $\varphi_{s\beta}^*$ of the reference are given by the following equation:

$$\begin{cases} \varphi_{s\alpha}^* = \left|\varphi_s^*\right| \cos\left(\theta_s^*\right) \\ \varphi_{s\beta}^* = \left|\varphi_s^*\right| \sin\left(\theta_s^*\right) \end{cases} \tag{26}$$

The components $V_{s\alpha}^*$ and $V_{s\beta}^*$ of the voltage vector are expressed below:

$$\begin{cases} V_{s\alpha}^* = \dfrac{\varphi_{s\alpha}^* - \varphi_{s\alpha}}{T_e} + R_s i_{s\alpha} \\ V_{s\beta}^* = \dfrac{\varphi_{s\beta}^* - \varphi_{s\beta}}{T_e} + R_s i_{s\beta} \end{cases} \tag{27}$$

Finally, the obtained components presented in (27) are used in the SVM block to determine the states $(S_a S_b S_c)$ of the inverter.

3. Design of DTC approaches from XSG

The XSG is a design and configuration tool of the Xilinx FPGAs, developed by Xilinx, and uses the Simulink of the Matlab environment [52]. The XSG design flow utilizing an FPGA is given as follows:

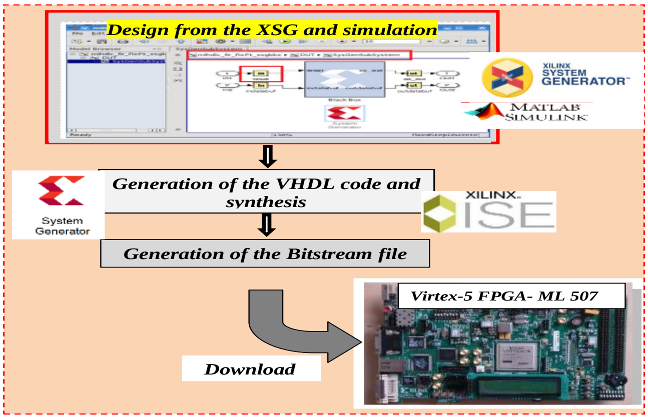

Fig. 12. XSG design flow

The first step of the design flow is to design the MPPT control algorithm, the basic DTC and the DTC-SVM from the XSG and then to verify the functionality of the system by simulation. The architecture is composed of several blocks and subsystems. In this section some blocks are presented by the following figures. Referring to equation (6), the internal architecture of the Concordia transformation block of the stator current is represented in Fig. 13.

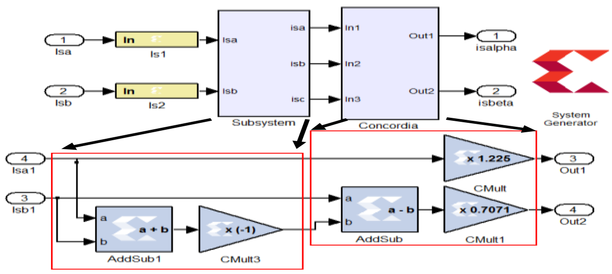

Fig. 13. Architecture of Concordia transformation of stator current from XSG

Referring to equation (7), the architecture of the stator flux components is depicted in Fig. 14.

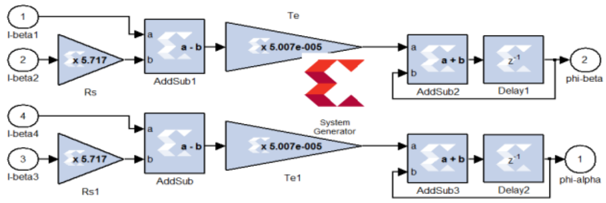

Fig. 14. Architecture of stator flux estimator from XSG

Referring to equation (8), the architecture of the Concordia transformation of the voltage vector is illustrated in Fig. 15.

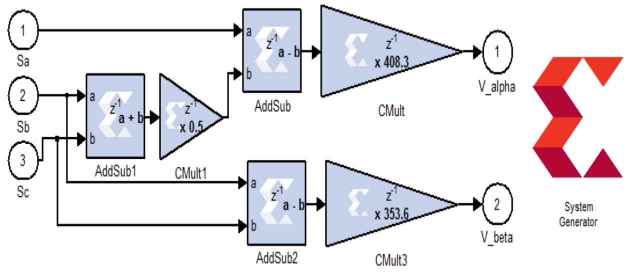

Fig. 15. Design of Concordia voltage block from XSG

Referring to Table 1, the internal architecture of switching table from the XSG is presented by in Fig. 16.

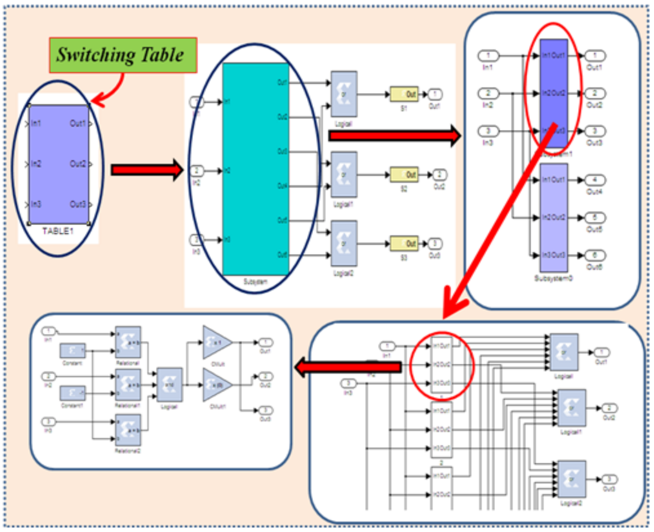

Fig. 16. Design of switching table from XSG

4. Simulation results and hardware implementation

4.1. Simulation results from XSG

In order to show the effectiveness of the DTC-SVM based on PI controllers relative to the basic DTC, the systems indicated in Fig. 1 and Fig. 2 are designed from the XSG and verified by digital simulation. The IM parameters are given in the Appendix. The reference of the stator flux is $\varphi_{sref} = 0.91wb$. In this step, the rotor reference speed is applied at t=0.12s, which is of 50 rd/s, then it increases to reach 100 rad/s and 150 rad/s at t=0.8 s and t=1.5s, respectively. The solar irradiation value is equal to 1000 W/m2. The temperature value is equal to 25 °C. The MPPT algorithm used in this paper is the P&O [43].The load torque applied by the pump is proportional to the square of the rotor speed [53], as demonstrated by the following equation:

$$T_l = k_l \Omega_m^2 \tag{28}$$

The parameters of the of the boost converter are shown in Table 2.

Table 2. The Boost converter parameters used in simulation

Parameters	*Values*
Output voltage	500 V
Output capacitance	37 µF
Inductance	21 mH
Switching frequency	10 kHz
Output voltage ripple (ΔV_o)	5%
Inductor current ripple (ΔI_L)	10%

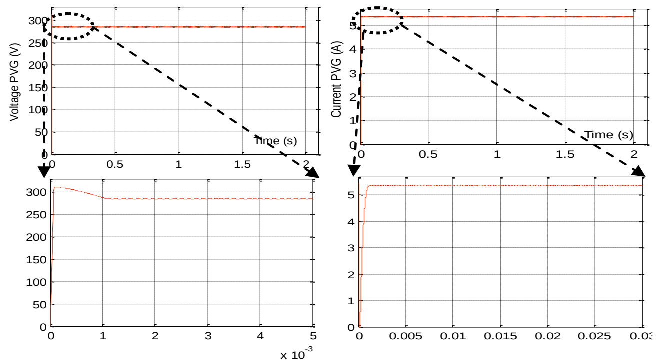

(a) (b)

Fig. 17. (a): Voltage and (b): current of PVG

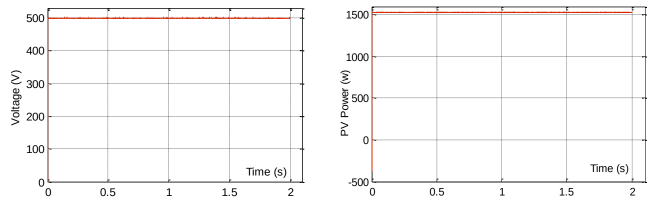

(a) (b)

Fig. 18. (a): Output voltage of the boost converter and (b): Power of the PVG

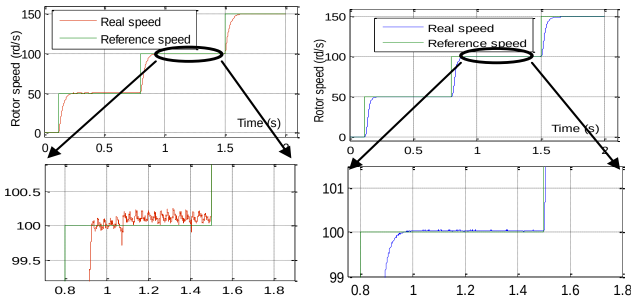

(a) (b)

Fig. 19. Evolution of rotor speed: (a) Basic DTC, (b) DTC-SVM

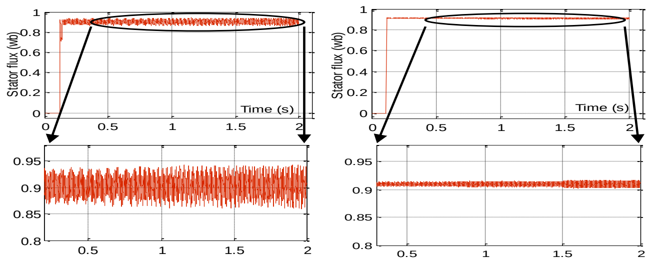

(a) (b)

Fig. 20. Evolution of stator Flux: (a) Basic DTC, (b) DTC-SVM

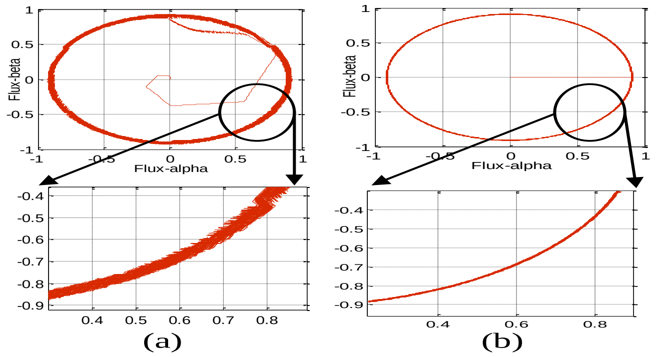

Fig. 21. Evolution of stator flux vector trajectory: (a) Basic DTC, (b) DTC-SVM

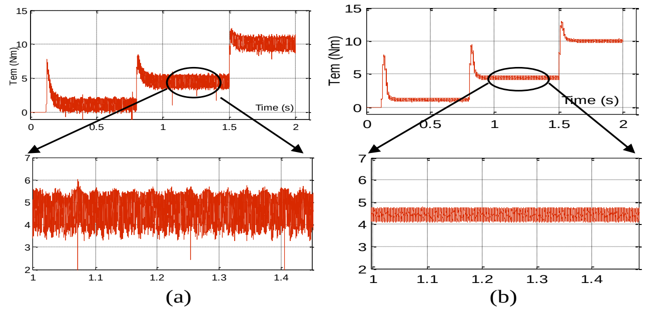

Fig. 22. Evolution of electromagnetic torque: (a) Basic DTC, (b) DTC-SVM

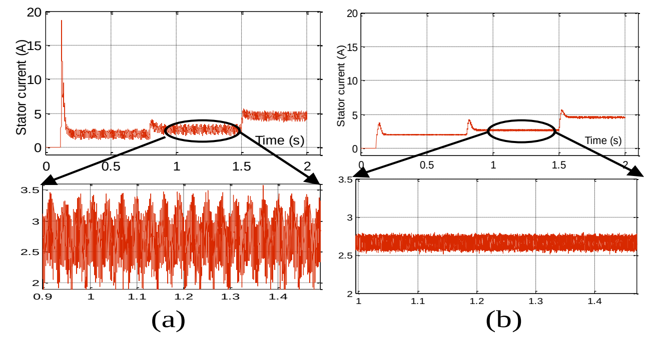

Fig. 23. Evolution of stator current module: (a) Basic DTC, (b) DTC-SVM

- *Discussion of the obtained results:*

The evolution of the voltage Vpv and the current Ipv provided by the PV generator are illustrated in Fig. 17.

Fig. 18(b) and Fig.18 (b) demonstrate the evolution of the output voltage of the chopper which is equal to 500 Vdc, and the PVG power, which is equal to 1500 w.

As shown in Fig.19, the IM operates with different reference speeds. In both control approaches, the basic DTC and DTC-SVM-based PI controllers, the rotor speed has quickly reached its reference value thanks to the high dynamics of the DTC. Nevertheless, in the basic DTC, the rotor speed possesses some ripples which are negligible in the DTC-SVM-based PI controllers.

Referring to Fig. 20 (a), Fig. 21 (a) and Fig. 22 (a), the stator flux and the electromagnetic torque possess high ripples due to the variation of the switching frequency in the basic DTC. These ripples are enormously reduced in the DTC-SVM thanks to the operation with a constant switching frequency, as shown in Fig. 20 (b), Fig. 21 (b) and Fig. 22 (b).

Referring to Fig. 23, the stator current distortion has been enormously reduced in the DTC-SVM

The performances of the DTC-SVM with the PI controllers in terms of ripples and harmonic distortions are summarized in the following table.

Table 3. Basic DTC and DTC-SVM A comparative study

	Basic DTC	*DTC-SVM based PI controllers*
	Max-Min	Max-Min
Electromagnetic torque ripples (Nm)	1.8	0.6
Stator flux ripples (wb)	0.045	0.009
Stator current distortions (A)	1.5	0.24

4.2. Hardware co-simulation

Hardware co-simulation using the XSG consists in integrating a design in an FPGA directly into a Simulink environment [54]. The Matlab/Simulink is utilized to design the power system that comprises the PV generator, the boost converter, the two-level inverter and the IM. The basic DTC, the DTC-SVM based PI controllers and the MPPT algorithm are realized through the XSG blockset. In the first step, the system was verified by digital simulation as presented in section 4 (4.1). In the second step the VHDL was been automatically generated and viewed by an RTL schematic and synthesized using the Xilinx ISE tool, as shown in Fig.24. Then, the control algorithm functionality was checked and it was ready for the hardware co-simulation. The hardware co-simulation step consists in: i) generating a JTAG bloc as given in Fig.25, ii) connecting the FPGA to PC computer through the JTAG cable, and then clicking on start simulation, hence the FPGA board exchanging the data with a full synchronization with the Simulink. In this step, the FPGA receives the stator current and the rotor speed, and after that sends the inverter switching states to Simulink through the JTAG cable, as represented in Fig.26.

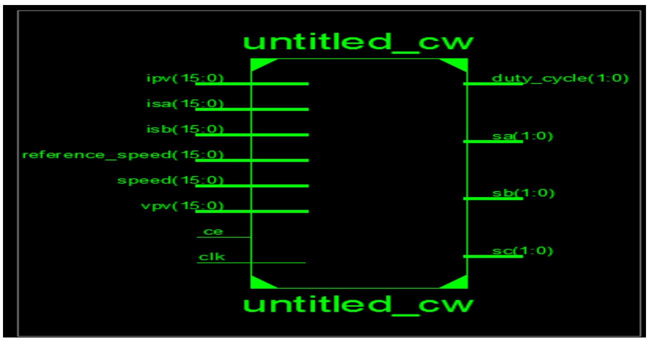

Fig. 24. RTL schematic of full control algorithm from Xilinx ISE 12.4

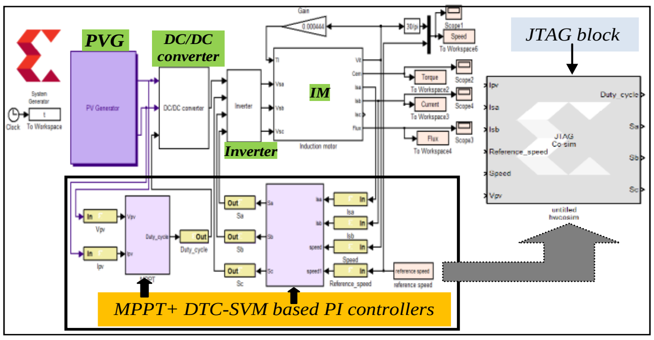

Fig. 25. Generation of JTAG hardware co-simulation step

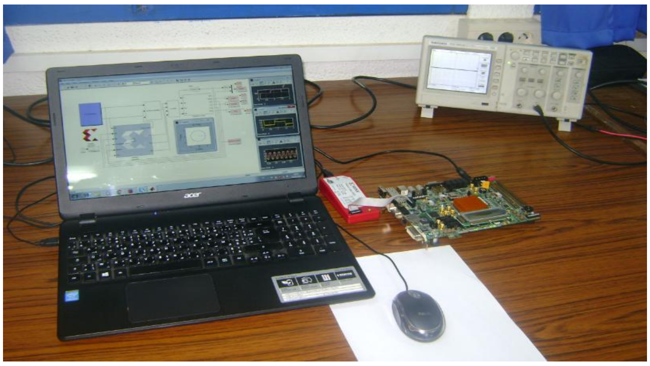

Fig. 26. Hardware co-simulation step for MPPT+DTC-SVM-based PI controllers

In the hardware co-simulation step, the induction motor response is presented by the following results, as given by Fig. 27 and Fig.28. The obtained co-simulation results are similar to those obtained by simulation. In this step, the rotor reference speed is applied at t=0.1s, which is of 100 rd/s. Next, it increases at t=0.8 s to reach 150 rad/s. After that, it decreases at t=1.5 to reach 100 rad/s. The solar irradiation value is equal to 1000 W/m2. The temperature value is equal to 25 °C.

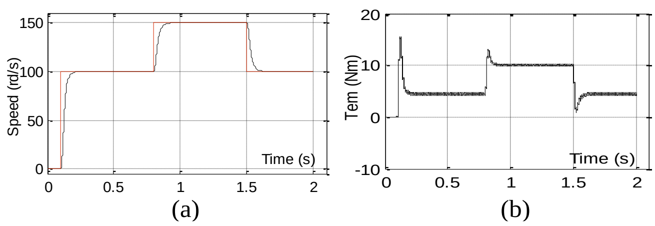

Fig. 27. Evolution of : (a) Rotor speed, (b) electromagnetic torque

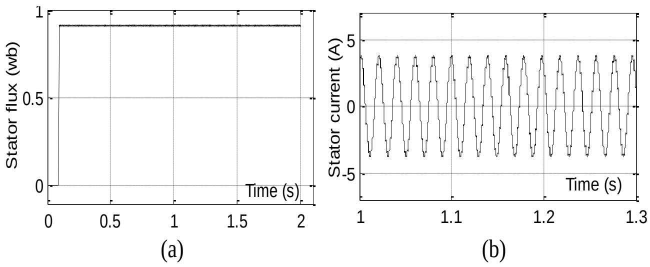

Fig. 28. Evolution of : (a) stator flux, (b) stator current

The consumed resources and the obtained timing FPGA performances of the designed DTC-SVM-based PI controllers and the MPPT algorithm hardware architecture are archived in Table 5.

Table 4. FPGA timing performances of DTC-SVM-PI and MPPT algorithms

Modules	***Computation time (µs)***
MPPT algorithm	T_{MPPT} =0.16
Concordia	T_{con}= 0.06
Stator Flux Estimator	T_{SFE}= 0.1
Electromagnetic Torque Estimator	T_{ETE} =0.06
Torque PI controller	T_{PI} =0.12
Calculation of the Stator Flux Reference	T_{SFR} =0.06
Calculation of the Voltage Vector Components	T_{VVC} =0.12
SVM	T_{SVM} =0.14
Execution Time of DTC-SVM-PI+MPPT	0.82 µs
Total control time of DTC-SVM-PI+MPPT	T_{ADC}+ 0.82
Consumed resources	25%

As shown in Table 5, the execution time of the full control algorithm is of (T_{ADC1}+ T_{ADC2} +0.82) µs, where T_{ADC1} and T_{ADC2} are the analog-to-digital conversion time of (I_{pv}, V_{pv}) and (U_{dc}, i_{sa}, i_{sb}), respectively. Therefore, the high capability of the FPGAs allows obtaining a low execution time, which consequently reduces the stator current distortion and harmonic waves. The benefits of the low execution time are discussed in paper [39]. In the paper of [55], the execution time is of 50 µs using the digital device dSPACE1104. The FPGA offered a low execution time relative to the dSPACE, thanks to its parallel computation. To sum up, Fig.29, presents the timing diagram of the control architecture illustrated in Fig.25.

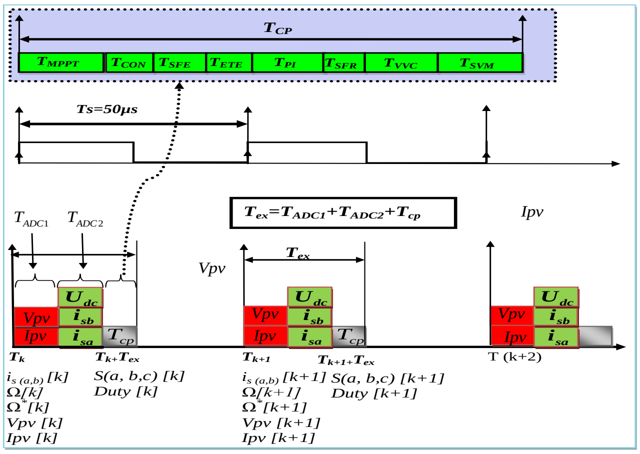

Fig. 29. Timing Diagram for implementation on FPGA

The total computation time T_{CP} is given by the following equation:

$$T_{CP} = T_{SFE} + T_{ETE} + T_{PI} + T_{SFR} + T_{VVC} + T_{SVM} = 0.82\mu s \qquad (29)$$

To determine the total execution time, the analog-to-digital conversion time must be added, as indicated in the following equation:

$$T_{ex} = T_{ADC1} + T_{ADC2} + T_{CP} \quad (30)$$

Referring to equation (30), the execution time depends firstly on T_{CP} which is very low, thanks to the parallel processing of the FPGA. It depends also on the analogue-to-digital conversion times TADC1 and TADC2. In order to get a control with a low execution time, it is important to choose an analogue converter with a low conversion time. Using an FPGA Virtex 5, we utilized a few resources, compared to the available potential. In the industrialization step, it is possible to choose an FPGA with fewer resources, thus having a lower cost.

The main differences between the MPPT algorithms are especially limited in the simplicity of the design, the convergence speed, the analog or digital implementation and the number of sensors, the PV array dependence, and the costs of the hardware. Thus, the good choice of the MPPT algorithm is too important for the user, because it increases the PV system efficiency, which consequently reduces the PV system costs by decreasing the number solar panels needed to get the desired power. A comparative study in terms of convergence speed, implementation complexity, sensor requirement and PV array dependence between some MPPT algorithms is archived in Table 6.

Table 5. A Comparative study between different MPPT algorithms

MPPT technique		PV array dependence	Analog/ digital	Convergence speed	Implementation complexity	Sensor
1	P&O [***56-59***]	No	Both	Vary	Low	V and I
2	Incremental conductance [***57, 58, 60-62***]	No	Digital	Vary	Medium	V and I
3	Fractional Voc [***58, 59, 29***]	Yes	Both	Medium	Low	V
4	Fractional Isc [***58, 59, 29***]	Yes	Both	Medium	Medium	V
5	Fuzzy logic control [63- ***65, 28***]	Yes	Digital	Fast	High	Varies
6	Neural network [58***, 63***]	Yes	Digital	Fast	High	Varies
7	genetic algorithms [30]	Yes	Digital	Fast	Moderate	V and I
8	Artificial neural network (ANN) based P&O MPPT [***58, 66***]	No	Both	High	Medium	V and I
9	Modified IC algorithm [***67***]	No	Digital	Medium	High	V and I
10	PSO [68]	No	Digital	High	Moderate	V and I

Referring to Table 6, the P&O method is less effective in terms of speed convergence relative to the FLC, the ANN, and the Modified IC algorithm. However in return, it is featured by its simplicity of implementation using the analog or the digital circuits, it is independent of the PV array characteristics, and does not require the measurement of the cell temperature and the solar intensity. These points favor its utilization in several applications [23, 33]. The IC has been developed to overcome the P&O limitation [69]. It is known as the best algorithm which is based on the disturbance and observation principle. The IC is featured by a fast dynamic response under rapid variations of the solar irradiances, but in return it is complex in implementation due to the calculation of derivatives [23]. A comparative between the P&O and IC algorithms, in terms of efficiency, is presented and discussed in paper [22] and shown in Table 7.

Table 6. Comparison in terms of efficiency between the P&O and IC techniques [22]

MPPT Technique	*Average efficiency : P_{out}/P_{max}*
P&O	97.58 %
IC	98.53 %

In paper [70], the average efficiencies of the IC and the HC algorithms were equal to 96.46% and 96.40 %, respectively. The genetic algorithm is featured by a good rapidity and accuracy, but the main limitation of this algorithm is that it is based on the panel model parameters that are not exactly equal to real panel parameters [30]. The PSO offers a good performance in terms of speed convergence, but it is more complex relative to the IC [68].

5. Conclusion

The target of this paper is firstly to develop DTC-SVM-based PI controllers and an MPPT control algorithm, as two control approaches of a pumping photovoltaic system. A comparative study between the classical DTC and the DTC-SVM has been carried out. Furthermore, a comparison between some MPPT algorithms has been discussed. The digital simulation from the XSG has shown that the DTC-SVM offers the best results in terms of torque ripples, flux ripples and stator current distortion. Secondly, the design of the suggested approaches has been verified by simulation from the XSG, and then the VHDL code has been generated, which can be used to generate the bitstream file and configure the FPGA. Before proceeding to a real system, the control algorithm bas been also verified, utilizing the FPGA board in the co-simulation step. Finally, a comparative study between the FPGA and the dSPACE has been performed. This study shows the FPGA performances in terms of execution time which is very weak relative to the dSPACE, consequently reducing the commutation losses of the inverter.

Appendix

Induction machine parameters	
Number of pairs of poles= 2 Rated frequency =50 Hz Rated voltage = 220/380 V Stator resistance = 5,717 Ω Rotor resistance= 4,282 Ω	Stator inductance =464mH Rotor inductance =464mH Mutual inductance =441,7mH Moment of inertia =0.0049 kg.m² Viscous friction coefficient =0.0029kg.m²/s

References

[1] R. Parajuli, G. Pokharel, and P. Østergaard, "A comparison of diesel, biodiesel and solar pv-based water pumping systems in the context of rural nepal," *International Journal of Sustainable Energy*, vol. 33, no. 3, pp. 536–553, 2014.

[2] C. Gopal, M. Mohanraj, P. Chandramohan, and P. Chandrasekar, "Renewable energy source water pumping systems a literature review," *Renewable and Sustainable Energy Reviews*, vol. 25, pp. 351 – 370, 2013.

[3] Rakesh Parekh, "AC Induction Motor Fundamentals", Microchip Technology Inc, AN887, DS00887A, pp 1-24, 2003.

[4] P. Periasamy, N.K. Jain and I.P. Singh, "A review on development of photovoltaic water pumping system," Renewable and Sustainable Energy Reviews, vol. 43, pp. 918-925, 2015.

[5] Habetler TG, Profumo F, Pastorelli M, Tolbert LM. Direct torque control of induction machines using space vector modulation. IEEE Transactions on Industry Applications, vol. 28, n°.5, pp. 1045-1053, 1992.

[6] Khoucha F, Lagoun SM, Marouani K, Kheloui A, El Hachemi Benbouzid M. Hybrid Cascaded H-Bridge Multilevel-Inverter Induction-Motor-Drive Direct Torque Control for Automotive Applications. IEEE Transactions on Industrial Electronics, vol. 57, n°.3, pp. 892-899, 2010.

[7] H. I. Okumus and M. Aktas, "Adaptive Hysteresis Band Control for Constant Switching Frequency in Direct Torque Control of Induction Machine Drives", Elec. Eng. & Comp. Sci. , vol 18, no. 1, pp.59-69, 2010.

[8] Zaimeddine R, Undeland T. DTC control schemes for induction motor fed by three-level NPC-VSI using space vector modulation. International Symposium on Power Electronics Electrical Drives Automation and Motion (SPEEDAM): IEEE. pp. 966-971, 2010.

[9] A. Abbou , H. Mahmoudi, "Performance of a sensorless speed control for induction motor using DTFC strategy and intelligent techniques," Journal of Electrical Systems, vol. 5, n°.3, 2009.

[10] S. Krim, S. Gdaim, A. Mtibaa and M.F. Mimouni, "Design and Implementation of Direct Torque Control Based on an Intelligent Technique of Induction Motor on FPGA". J Electr Eng Technol., vol. 10, n°.4, pp. 1527-1539, 2015.

[11] A.R. Reisi, M.H. Moradi, S. Jamasb, Classification and comparison of maximum power point tracking techniques for photovoltaic system: a review, Renew. Sustain. Energy Rev., vol. 19, pp.433–443, 2013.

[12] Babu, T. Sudhakar, N. Rajasekar, and K. Sangeetha. "Modified particle swarm optimization technique based maximum power point tracking for uniform and under partial shading condition." *Applied Soft Computing* 34, pp. 613-624, 2015.

[13] T. Esram, J.W. Kimball, P.T. Krein, P.L. Chapman, P. Midya, Dynamic maximum power point tracking of photovoltaic arrays using ripple correlation control, IEEE Trans. Power Electron, vol. 21, pp. 1282–1291, 2006.

[14] K. Ishaque, Z. Salam, A review of maximum power point tracking techniques of PV system for uniform insolation and partial shading condition, Renew. Sustain. Energy Rev., vol. 19, pp. 475–488, 2013.

[15] T. Noguchi, S. Togashi, R. Nakamoto, Short-current pulse-based maximum-power-point tracking method for multiple photovoltaic-and converter module system, IEEE Trans. Ind. Electron., vol. 49, pp. 217–223, 2002.

[16] K. Kobayashi, H. Matsuo, Y. Sekine, A novel optimum operating point tracker of the solar cell *power supply system, in: Proceedings' 35th Annual IEEE Power Electronics Specialists Conference*, pp. 2147–2151, 2004.

[17] M.A. Masoum, H. Dehbonei, E.F. Fuchs, Theoretical and experimental analyses of photovoltaic systems with voltage and current-based maximum power point tracking, IEEE Power Eng., vol. 22, pp. 62–72, 2002.

[18] A.G.B. Moacyr, L. Galotto, L.P. Sampaio, A.M. Guilherme, Evaluation of the main MPPT techniques for photovoltaic applications, IEEE Trans. Ind. Electron., vol. 60, pp. 1156–1167, 2013.

[19] M.A. Elgendy, B. Zahawi, Assessment of perturb and observe MPPT algorithm implementation techniques

for PV pumping applications, IEEE Trans. Solar Energy, vol. 3, pp. 21–33, 2012.

[20] N. Femia, G. Petrone, G. Spagnuolo, M. Vitelli, Optimization of perturb and observe maximum power point tracking method, IEEE Trans. Power Electron. , vol. 20, pp. 963–973, 2005.

[21] A.K. Abdelsalam, A.M. Massoud, S. Ahmed, High-performance adaptive perturb and observe MPPT technique for photovoltaic-based microgrids, IEEE Trans. Power Electron, vol. 26, pp. 1010–1021, 2011.

[22] Fernando Lessa Tofoli, Dênis de Castro Pereira, and Wesley Josias de Paula, Comparative Study of Maximum Power Point Tracking Techniques for Photovoltaic Systems. International Journal of Photoenergy, pp.1-10, 2015.

[23] X. Zhou, D. Song, Y. Ma, The simulation and design for MPPT of PV system based on incremental conductance method, in: Information Engineering (ICIE), 2010 WASE International Conference, 2010, pp. 314–317.

[24] L. Jae, B. HyunSu, C. Bo Hyung, Advanced incremental conductance MPPT algo-rithm with a variable step size, in: 12th International Power Electronics and Motion Control Conference, 2006 EPE-PEMC '06, pp. 603–607, 2006.

[25] S. Mekhilef Safari, Simulation and hardware implementation of incremental conductance MPPT with direct control method using cuk converter, IEEE Trans. Ind. Electron., vol. 58, pp. 1154–1161, 2011.

[26] Sangeetha, K., T. Sudhakar Babu, and N. Rajasekar. "Fireworks Algorithm-Based Maximum Power Point Tracking for Uniform Irradiation as Well as Under Partial Shading Condition." Artificial Intelligence and Evolutionary Computations in Engineering Systems. Springer India, pp. 79-88, 2016.

[27] X. Weidong, W.G. Dunford, A modified adaptive hill climbing MPPT method for photovoltaic power systems, in: IEEE Power Electronics Specialists Conference, vol. 35, pp. 1957–1963, 2004.

[28] Takun, P., Kaitwanidvilai, S., & Jettanasen, C. Maximum power point tracking using fuzzy logic control for photovoltaic systems," presented at International Multi Conference of Engineers and Computer Scientists, Hong Kong, vol. 2, 2011.

[29] Kumari, J., & Babu, Ch. Comparison of maximum power point tracking algorithms for photovoltaic system. International Journal of Advances in Engineering and Technology, vol. 1, pp. 133–148, 2011.

[30] Slimane HADJI, Jean-Paul GAUBERT and Fateh KRIM. Experimental analysis of genetic algorithms based MPPT for PV systems. International Renewable and Sustainable Energy Conference (IRSEC), pp. 7 – 12, 2014.

[31] Babu, T. Sudhakar, K. Sangeetha, and N. Rajasekar. "Voltage band based improved particle swarm optimization technique for maximum power point tracking in solar photovoltaic system."Journal of Renewable and Sustainable Energy, vol. 8, n°. 1, pp. 2016.

[32] D. Hohm and M. Ropp, "Comparative study of maximum power point tracking algorithms using an experimental, programmable, maximum power point tracking test bed," in Proceedings of the 28th IEEE Photovoltaic Specialists Conference, pp. 1699–1702, IEEE, Anchorage, Alaska, USA, 2000.

[33] Y. Huang, M. Shen, F. Z. Peng, and J. Wang, "A Z-source inverter for residential photovoltaic systems," IEEE Transactions on Power Electronics, vol. 21, no. 6, pp. 1776–1782, 2006.

[34] Mohammed A. Elgendy, Bashar Zahawi, and David J. Atkinson, Assessment of Perturb and Observe MPPT Algorithm Implementation Techniques for PV Pumping Applications. IEEE TRANSACTIONS ON SUSTAINABLE ENERGY, VOL. 3, NO. 1, JANUARY 2012.

[35] T. Esramand P. L.Chapman, "Comparison of photovoltaic array maximumpower point tracking techniques," IEEE Transactions on Energy Conversion, vol. 22, no. 2, pp. 439–449, 2007.

[36] Motor control with STM32®32-bit ARM®-based MCU. Pdf. http://www.st.com/web/en/ resource/sales_ and_marketing /promotional_material/brochure/brstm32mc.pdf.

[37] A. Hmidet, R. Dhifaoui and O. Hasnaoui, "Development, Implementation and Experimentation on a dSPACE DS1104 of a Direct Voltage Control Scheme", Journal of Power Electronics, Vol. 10, N°.5, pp. 468-476, 2010.

[38] L. Idkhajine, E. Monmasson, M. W. Naouar, A. Prata, and K. Bouallaga. Fully Integrated FPGA-Based Controller for Synchronous Motor Drive. IEEE TRANSACTIONS ON INDUSTRIAL ELECTRONICS, VOL. 56, NO. 10, OCTOBER 2009.

[39] M.W. Naouar, E. Monmasson, A. A. Naassani, I. S. Belkhodja, and N. Patin. FPGA-Based Current Controllers for AC Machine Drives—A Review. IEEE TRANSACTIONS ON INDUSTRIAL ELECTRONICS, VOL. 54, NO. 4, AUGUST 2007.

[40] Xilinx Inc. System Generator for DSP User Guide, December 2010

[41] M. Villalva, J. Gazoli, and E. Filho, "Comprehensive approach to modeling and simulation of photovoltaic arrays," *Power Electronics, IEEE Transactions on*, vol. 24, pp. 1198–1208, May 2009.

[42] M. Bahloul, L. Chrifi-Alaoui, M. Souissi, M. Chaabane, S. Drid, Effective Fuzzy Logic Control of a Stand-alone Photovoltaic Pumping System, *international journal of renewable energy research*, Vol.5, No.3, 2015.

[43] M. Dris, B. Djilani, "Comparative Study of Algorithms (MPPT) Applied to Photovoltaic Systems", International Journal of Renewable Energy Research, Vol.3, No.4,14 November 2013.

[44] Tarak Salmi, Mounir Bouzguenda, Adel Gastli and Ahmed Masmoudi, MATLAB/Simulink Based Modelling of Solar Photovoltaic Cell, International journal of renewable energy research, Vol.2, No.2, 2012.

[45] S.Choudhury, P.K.Rout. Adaptive Fuzzy Logic Based MPPT Control for PV System under Partial Shading

Condition. International journal of renewable energy research, vol.5, N°.4, 2015.

[46] C. Ben Salah, M. Ouali, “Comparison of fuzzy logic and neural network in maximum power point tracker 713 for PV systems”, Electric Power Systems Research, Vol.81, pp. 43-50, January 2011.

[47] K. Chomsuwan, Ladkrabang, P. Prisuwanna, V. Monyakul. Photovoltaic grid-connected inverter using two-switch buck-boost converter. Photovoltaic Specialists Conference. Conference Record of the Twenty-Ninth IEEE, 2002.

[48] X. Liu, L. A. C. Lopes. An improved perturbation and observation maximum power point tracking algorithm for PV arrays. Power Electronics Specialists Conference. PESC 04. 2004 IEEE 35th Annual, pp.1957-1963, 2004.

[49] Takahashi I, Noguchi T. A New Quick-Response and High-Efficiency Control Strategy of an Induction Motor. IEEE Transactions on Industry Applications, IA-22:820-827, 1986.

[50] J. Holtz, “Pulse width modulation for electronic power conversion,” *IEEE Proc.*, vol. 82, pp. 1194-1213, 1994.

[51] W. Srirattanawichaikul Y. Kumsuwan and S. Premrudeepreechacharn. Reduction of torque ripple in direct torque control for induction motor drives using decoupled amplitude and angle of stator flux control. ECTI Transactions On Electrical Engineering, Electronics, and Communications, 8(2):187–196, August 2010.

[52] http://www.xilinx.com/support/sw_manuals/sysgen_gs. pdf.

[53] B. Kumar, Y. K. Chauhan, and V. Shrivastava, “A comparative study of maximum power point tracking methods for a photovoltaic-based water pumping system,” *International Journal of Sustainable Energy*, vol. 33, no. 4, pp. 797–810, 2014.

[54] http://www.tkn.tu-berlin.de/fileadmin/ fg112/Papers /chwalisz2011hwcosim.pdf.

[55] Abdesslam Lokriti, Issam Salhi, and Said Doubabi. IM Direct Torque Control with no flux distortion and no static torque error. ISA Transactions, vol. 59, pp. 256-267, 2015.

[56] Sera, D., Kerekes, T., Teodorescu, R., & Blaabjerg, F. (2006b). “Improved MPPT Algorithms for Rapidly Changing Environmental Conditions,” presented at Power Electronics and Motion Control Conference, 2006. EPE-PEMC, pp. 1614–1619.

[57] Jusoh, A., Sutikno, T., Guan, T. K., & Mekhilef, S. A Review on favourable maximum power point tracking systems in solar energy application. *Telkomnika, vol. 12, n°.* 1, pp. 6–22, 2014.

[58] Kamarzaman, N., & Tan, C. W. A comprehensive review of maximum power point tracking algorithms for photovoltaic systems. Renewable and Sustainable Energy Reviews, vol. 37, pp. 585–598, 2014.

[59] Busa, V., Narsingoju, K. K., & Kumar, G. V. Simulation analysis of maximum power control of photo voltaic power system. International Journal on Advanced Electrical and Electronics Engineering (IJAEEE), vol. 1, n°.1, pp.9–14, 2012.

[60] Yadav, A., Thirumaliah, S., & Haritha, G. Comparison of MPPT algorithms for DC–DC converters based PV systems. International Journal of Advanced Research in Electrical, Electronics and Instrumentation Engineering, vol. 1, pp. 18–23, 2012.

[61] Rashid, M. H. (2011). Power Electronic Handbook (3rd ed.). USA: Butterworth-Heinemann.

[62] Zainudin, H., & Mekhilef, S. “Comparison study of maximum power point tracker techniques for PV systems,” presented at international middle east power systems conference (MEPCON’10) (pp. 750–755). Egypt: Cairo University, 2010.

[63] Ali, A., Saied, M., Mostafa, M., & Moneim, T. A survey of maximum PPT techniques of PV Systems. Energytech, IEEE 2012.

[64] Rezaei, A., & Gholamian, S. A. Optimization of New Fuzzy Logic Controller by Genetic Algorithm for Maximum Power Point Tracking in Photovoltaic System. Journal of Science and Technology, vol. 9, n°1, pp. 9–16, 2013.

[65] Rahmani, R., Seyedmahmoudian, M., Mekhilef, S., & Yusof, R. Implementation of fuzzy logic maximum power point tracking controller for photovoltaic system. American Journal of Applied Sciences, vol. 10, pp.209–218, 2013.

[66] Amrouche, B., Belhamel, M., & Guessoum, A. ”Artificial intelligence based P&O MPPT method for photovoltaic systems,” Revue des Energies Renouvelables ICRESD, Vol. 7, pp. 11–16, 2007.

[67] Mastromauro, R., Liserre, M., & Aquila, A. Control issues in single-stage photovoltaic systems: MPPT, current and voltage control. IEEE Transactions on Industrial Informatics, vol.8, n°.2, pp. 241–254, 2012.

[68] Mohammadmehdi Seyedmahmoudian, Rasoul Rahmani, ,Saad Mekhilef, Amanullah Maung Than Oo, Alex Stojcevski, Tey Kok Soon, and Alireza Safdari Ghandhari. Simulation and Hardware Implementation of New Maximum Power Point Tracking Technique for Partially Shaded PV System Using Hybrid DEPSO Method. IEEE TRANSACTIONS ON SUSTAINABLE ENERGY, VOL. 6, NO. 3, JULY 2015.

[69] K. H. Hussein, I. Muta, T. Hoshino, and M. Osakada, “Maximum photovoltaic power tracking: an algorithm for rapidly changing atmospheric conditions,” IEE Proceedings:Generation, Transmission and Distribution, vol. 142, no. 1, pp. 59–64, 1995.

[70] Sangeetha, K., et al. "Modeling, analysis and design of efficient maximum power extraction method for solar PV system." Sustainable Energy Technologies and Assessments, vol. 15, pp.60-70, 2016.